

## STUDY OF CONVECTIVE FLOW EFFECTS IN ENDWALL CASING TREATMENTS IN TRANSONIC COMPRESSOR ROTORS

Chunill HAH<sup>1</sup>, Martin MUELLER<sup>2</sup> and Heinz-Peter SCHIFFER<sup>2</sup>

<sup>1</sup>NASA Glenn Research Center,  
MS 5-11, Cleveland, Ohio 44135

<sup>2</sup>Technische Universität Darmstadt  
D-64287 Darmstadt, Germany

### ABSTRACT

The unsteady convective flow effects in a transonic compressor rotor with a circumferential-groove casing treatment are investigated in this paper. Experimental results show that the circumferential-groove casing treatment increases the compressor stall margin by almost 50% for the current transonic compressor rotor. Steady flow simulation of the current casing treatment, however, yields only a 15% gain in stall margin. The flow field at near-stall operation is highly unsteady due to several self-induced flow phenomena. These include shock oscillation, vortex shedding at the trailing edge, and interaction between the passage shock and the tip clearance vortex. The primary focus of the current investigation is to assess the effects of flow unsteadiness and unsteady flow convection on the circumferential-groove casing treatment. Unsteady Reynolds-averaged Navier-Stokes (URANS) and Large Eddy Simulation (LES) techniques were applied in addition to steady Reynolds-averaged Navier-Stokes (RANS) to simulate the flow field at near-stall operation and to determine changes in stall margin. The current investigation reveals that unsteady flow effects are as important as steady flow effects on the performance of the circumferential grooves casing treatment in extending the stall margin of the current transonic compressor rotor. The primary unsteady flow mechanism is unsteady flow injection from the grooves into the main flow near the casing. Flows moving into and out of the grooves are caused due to local pressure difference near the grooves. As the pressure field becomes transient due to self-induced flow oscillation, flow injection from the grooves also becomes unsteady. The unsteady flow simulation shows that this unsteady flow injection from the grooves is substantial and contributes significantly to extending the compressor stall margin. Unsteady flows into and out of the grooves have as large a role as steady flows in the circumferential grooves. While the circumferential-

groove casing treatment seems to be a steady flow device, unsteady flow effects should be included to accurately assess its performance as the flow is transient at near-stall operation.

### INTRODUCTION

Circumferential-groove casing treatments have been applied very successfully for certain subsonic and transonic compressors. Although it is generally believed that circumferential-groove casing treatments do extend stall margins for compressor rotors with tip loaded designs, the fundamental flow mechanisms are not fully understood. Furthermore, the design criteria of the circumferential grooves are mainly based on loosely connected experimental data from subsonic compressors. Precise understanding of the dominant flow mechanisms will result in better and faster design of casing treatments.

Many studies to investigate casing treatments in compressors have been reported (Moore et al. [1971], Prince et al. [1974], Paulon and Dehoudt [1982], Smith and Cumpsty [1985], Fujita and Takata [1985], Lee and Greitzer [1990], Crook et al. [1993], Hall et al. [1996], Rabe and Hah [2002], Shabbir and Adamczyk [2004], Chen et al. [2010], and Mueller et al. [2011]). Paulon and Dehoudt [1982] conducted a theoretical investigation of the effects of circumferential-groove casing treatments. Mueller et al. [2007] investigated various circumferential grooves applied to the rotor in a single-stage transonic compressor. Particle Imaging Velocimetry (PIV) was applied to measure the detailed steady flow field near and inside circumferential grooves in an axial transonic compressor stage by Mueller et al. [2011].

Although significant progress has been made in non-intrusive measurement techniques, direct measurements of steady and unsteady velocity components in the tip clearance region of high speed turbomachinery are still beyond current

capabilities. Therefore, numerical approaches have been used to investigate flow mechanisms in the tip clearance region in high speed compressors. Most previous numerical studies are based on the steady Reynolds-averaged Navier-Stokes (RANS) approach (Hall et al. [1996], Rabe and Hah [2002], Mueller et al. [2007], Chen et al. [2010]) It has been observed that the steady RANS approach calculates some effects of circumferential grooves on the stall margin even though the flow field itself is unsteady near stall. However, measured increases in stall margin are not well calculated with steady RANS.

Previous studies (for example, Prince et al. [1974]) identified the following possible effects of circumferential-groove casing treatments on flow near the end wall:

1. Effects on two-dimensional boundary layers near the blade tip.
2. Effects on tangential velocity and momentum components of tip clearance flow.
3. Effects on end wall boundary layers.
4. Effects on tip clearance vortex structures.

Previous studies on stall inception (for example, Vo et al. [2005]) reveal that short length scale stall inception occurs when a large flow blockage develops on the pressure side of the blade near the leading edge causing incoming flow to spill over to the adjacent blade passage. Mueller et al. [2007] showed that a large portion of this blockage is created by the tip clearance flow originating between 20% and 50% of the blade chord. Tip clearance flows originating between the leading edge and 20% chord form a tip clearance core vortex which travels radially inward. The tip clearance flows originating from 20% to 50% chord travel over this tip clearance core vortex to reach the pressure side of the adjacent blade. This part of the tip clearance flow has low momentum because it comes from the casing boundary layer and the blade suction-surface boundary layer. Part of the tip clearance flow near the casing moves into the grooves. Consequently, the buildup of the induced vortex and the blockage near the pressure side of the passage is reduced (Mueller et al. [2007]). Tangential momentum of the tip clearance flow is also reduced due to the grooves and the tip clearance vortex stays close to the blade suction side. These seem to be the main mechanisms of circumferential grooves in delaying the formation of blockage near the pressure side of the passage and the onset of short length scale stall inception.

Steady RANS flow simulations have been able to replicate some observed effects of circumferential grooves. However, it appears that RANS simulations (Mueller et al. [2007], Chen et al. [2010], and Van de Wyer et al. [2010]) do not capture all of the important flow mechanisms of the grooves. Previous studies show that RANS simulations do not calculate measured changes in stall margin reliably.

The present paper investigates the effects of unsteady flow convection on circumferential-groove casing treatments using URANS and LES methods. The primary motivation is the fact that circumferential-grooves casing treatments are intended to control compressor flow fields near the casing at near-stall operation. The inclusion of unsteady flow effects is

necessary because the flow field near the casing at near-stall operation is highly transient due to self-induced flow oscillation.

## TEST ROTOR WITH CIRCUMFERENTIAL-GROOVE CASING TREATMENT

Measured data from an axial, single-stage transonic compressor with a circumferential-groove casing treatment are used in the current investigation. The test rig at the University of Darmstadt, Germany has been used to test many different types of casing treatments using the latest measurement techniques for compressor flow research.

The design parameters of the high-speed test rig represent the front stage of a typical commercial HPC. The rig has been built for validation of design tools and CFD codes. It also functions as an experimental test bed for new materials and manufacturing methods such as blisks and CRP. The test facility operates in an open circuit; ambient air is sucked into a settling chamber and through a calibrated bell mouth into the stage. Due to the length of the inlet duct and the small volume established at the stage outlet, stall can occur but surge cannot.

The rotor used for all measurements presented herein is the Darmstadt Rotor-1 titanium blisk with 16 radially stacked CDA-profiles. Figure 1 shows the cross section of the single-stage axial compressor.

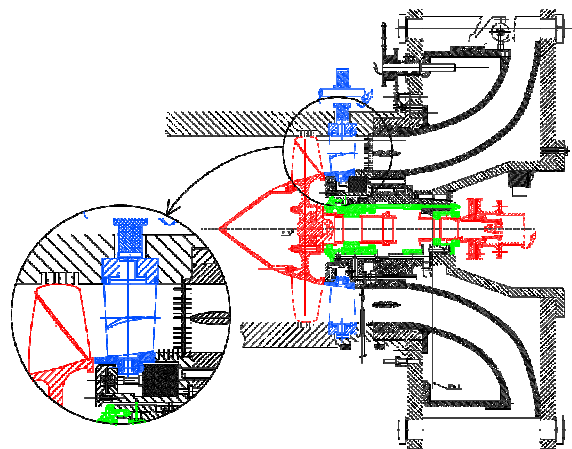


Figure 1: Cross section of transonic compressor stage.

Details of the test rotor and the groove configurations are given by Mueller et al. [2007]. Many different casing inserts were manufactured, each with a unique configuration of grooves. For the current study, the flow field with 6 deep grooves shown in Figure 2 is examined in detail. The grooves begin at 15.25% of the projected axial chord downstream of the leading edge with the groove depth of 12 mm and aspect ratio of 3. Probes inside the settling chamber are employed to identify the inlet flow conditions. For exit flow measurements, pressure and temperature rakes are mounted on the struts behind the stator. They are equipped with eleven radial sensors each. Therefore, all experimental results are related to the whole stage. Static wall pressure at the hub and tip is measured at the same axial position as the rakes.

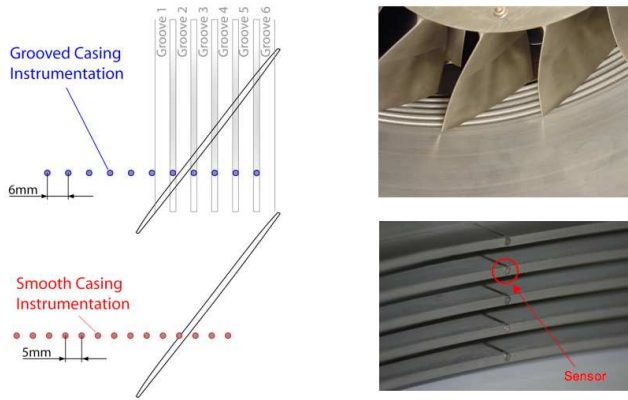


Figure 2: Compressor rotor with six deep grooves and instrumentation for the wall pressure measurement.

### NUMERICAL APPROACHES AND CFD GRID

The steady RANS, URANS and LES approaches were applied to obtain steady and unsteady flow fields at various operating conditions and to determine the operating range of the compressor rotor at design speed. The primary focus of the numerical analysis was to explain the flow mechanisms associated with the circumferential-groove casing treatment. Therefore, the isolated rotor configuration with circumferential grooves was analyzed numerically. The current compressor stage has a relatively large space between the rotor and the stator (40 % of rotor axial chord at mid-span), and the upstream influence of the stator flow field on the rotor flow field is believed to be relatively minor. The URANS solutions were used to obtain instantaneous flow structures at near-stall operation. A modified two-equation turbulence model was used for turbulence closure in the RANS and URANS methods. LES was applied to see if any additional changes in operating range occur with a more realistic description of the tip clearance vortex at near-stall operation (Hah et al. [2010]).

In the current study, the governing equations are solved with a pressure-based implicit method using a fully conservative control volume approach. A third-order accurate interpolation scheme is used for the discretization of convection terms and central differencing is used for the diffusion terms. The method is of second-order accuracy with smoothly varying grids. For the time-dependent terms, an implicit second-order scheme is used and a number of sub-iterations are performed at each time step. Details of the RANS method, turbulence closure, and applications to transonic flows are given by Hah and Wennerstrom [1990].

The computational grid for a single blade passage consists of 98 nodes in the blade-to-blade direction, 106 nodes in the spanwise direction, and 460 nodes in the streamwise direction. The inflow boundary is located 6 average blade heights upstream of the rotor leading edge, and the outflow boundary is located 6 blade heights from the trailing edge. The rotor tip clearance geometry is accurately represented by 18 nodes in the blade-to-blade direction, 16 nodes in the spanwise direction, and 340 nodes in the streamwise direction. The circumferential grooves were

modeled in a separated block. Each groove is represented by 98 nodes in the circumferential direction and 20 nodes in the radial and axial directions. The I-grid topology is used to reduce grid skewness, and a single-block grid is used. All computations were performed with NASA's Columbia super computer system, which allows parallel computation with up to 512 processors.

Standard boundary conditions for an isolated rotor were applied at the boundaries of the computational domain. Circumferentially averaged static pressure at the casing was specified to control the mass flow rate. Non-reflecting boundary conditions were applied at the inlet and the exit boundaries.

### MEASURED AND CALCULATED COMPRESSOR ROTOR OPERATING RANGES

Figure 3 compares changes in pressure rise and isentropic efficiency at design speed due to the casing treatment with six circumferential grooves from measurements, RANS, URANS, and LES. Measured flow characteristics show that the operating range increases by almost 50% with the circumferential-groove casing treatment. In Figure 3, calculated rotor performance is compared with the measured compressor stage performance. Isolated rotor performance was not measured due to the limitation of probe access. Some minor effects of the stator on the measured stage pressure rise and stage efficiency are estimated. It is believed that the relative effects of the circumferential grooves on the changes in stall margin are not influenced by the presence of the stator.

It is not easy to measure the exact stalling mass flow rate of a transonic compressor rotor. For this rotor, slightly different stalling mass flow rates have been observed experimentally with different measurement techniques. The currently reported stalling mass flow rate is repeatable and measurement error is estimated to be negligible. It is well known that the magnitude and actual shape of the tip clearance significantly affect the stall margin of any transonic compressor. Previous numerical analyses of this rotor used an estimated tip gap, which is about 20 % smaller than the recently measured value. The actual measured tip gap is used in the current numerical calculation and the calculated pressure rise characteristics with the actual tip gap are shown in Figure 3.

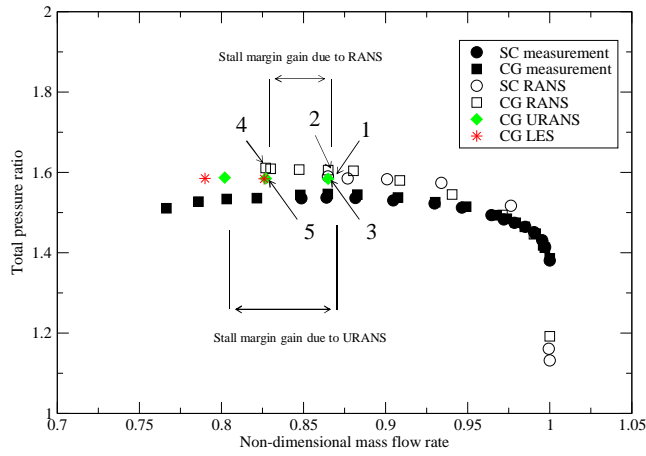


Figure 3(a): Total pressure rise at design speed.

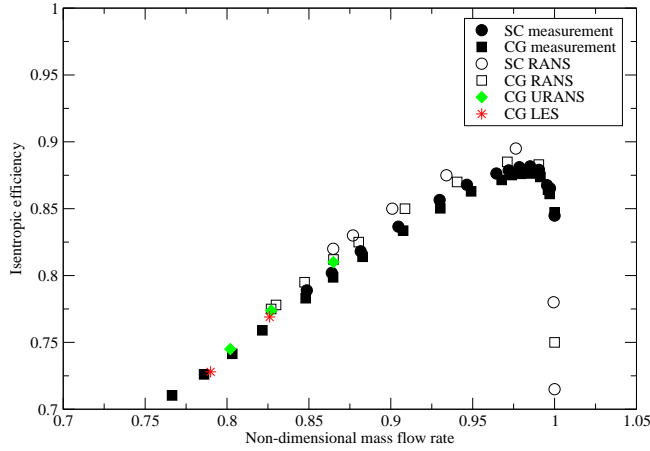
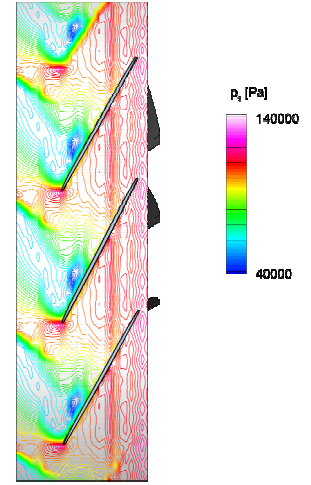
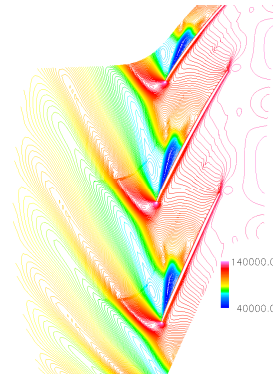


Figure 3(b): Isentropic efficiency at design speed.

Static pressure distributions at the stall limit with the smooth casing from RANS and from high-response pressure measurements are compared in Figure 4. The overall flow field and detailed shock structures are well calculated with the current numerical approach.



Measurement



RANS simulation

Figure 4: Comparison of flow structure at near-stall operation, smooth casing.

For the smooth casing without grooves, steady RANS calculates a stall mass flow rate somewhat higher than the measured value, giving a stall margin about 8% smaller than that from the measurements. As is well known, periodicity of the flow field across blade passages breaks down as the compressor rotor operates toward stall. Even at stable operation before stall, compressor rotors operate with drastically varying flow structure over multiple blade passages (for example, flow instability, Martz et al. [2001]). Single-passage steady RANS has been widely used to assess the stall mass flow rate and the stall margin of compressor rotor even though the flow field is unsteady and non-periodic at near stall operation. It appears that RANS calculates a slightly higher stall mass flow rate than measurements for most reported cases (for another example, Chen et al. [2010]). In the current study, single-passage steady and unsteady flow simulations are applied for both the smooth wall case and that with the circumferential-grooves casing treatment. Any possible multi-passage flow effects at near stall operation are not modeled with the current approach. For smooth casing, both RANS and URANS calculate almost identical stall mass flow rate for



this rotor and results with URANS for the smooth casing are not shown in Figure 3.

Calculated compressor operating ranges with circumferential grooves from RANS, URANS, and LES are shown in Figure 3. The calculated stall mass flow rate with steady RANS is much higher than the measured value, giving an increase in stall margin of 15% with the circumferential-groove casing treatment, compared to a measured increase of almost 50%. Previous numerical investigations (for example, Chen et al. [2010]) show a similar trend in calculating stall margin increase due to circumferential grooves with steady RANS. On the other hand, unsteady URANS calculates much lower stall mass flow rates than RANS. URANS simulation predicts almost 33% increase in stall margin, which is much closer to the measured value. These RANS and URANS simulations were performed with identical turbulence closures and computational grids. Therefore, the differences in calculated stall margins and mass flow rates are due to the unsteady effect of the flow field. In the following sections, unsteady flow effects are examined at mass flow rates at which the smooth-casing compressor stalls and at which the RANS simulation with the circumferential-groove casing treatment stalls.

#### EFFECTS OF STEADY AND UNSTEADY FLOW CONVECTION WITH THE CIRCUMFERENTIAL GROOVE CASING TREATMENT

When the compressor rotor operates near the stall condition, the flow field becomes highly unsteady due to self induced flow oscillation. Figure 5 shows axial velocity distributions from PIV measurements near stall at three different times (Hah et al. [2010]). Measured changes in pressure difference across the blade tip section near the leading edge at near stall operation with smooth casing are shown in Figure 6 (Bergner et al. [2006]). Large changes in pressure difference in Figure 6 indicate that the flow field is highly unsteady and the tip clearance flow is also highly transitional. The circumferential-groove casing treatment is designed to delay further deterioration of the flow field and to extend the stable operating range. To study why the URANS simulation with circumferential grooves calculates a lower stall mass flow than the RANS simulation as shown in Figure 3, calculated flow fields at the mass flow rate where the smooth-casing RANS simulation stalls are examined in detail.

Calculated axial velocity distributions just downstream of the blade trailing edge from RANS with the smooth casing, RANS with circumferential grooves (CG), and URANS with CG are compared in Figure 7. All the velocity units are meters per second. The results of URANS in Figure 7 are from the time-averaged solution. The axial velocity distribution in Figure 7 indicates a degree of aerodynamic blockage in the blade passage. The comparison in Figure 7 clearly shows that overall blockage is reduced with the CG casing treatment. Furthermore, blockage from URANS with the CG treatment is smaller than that from RANS with the CG treatment. The difference in blockage between URANS

and RANS with the CG treatment represents the effects of unsteady flow convection in the CG casing treatment. The difference in blockage between RANS with the smooth casing and RANS with the CG treatment represents the effects of steady flow convection in the CG casing treatment.

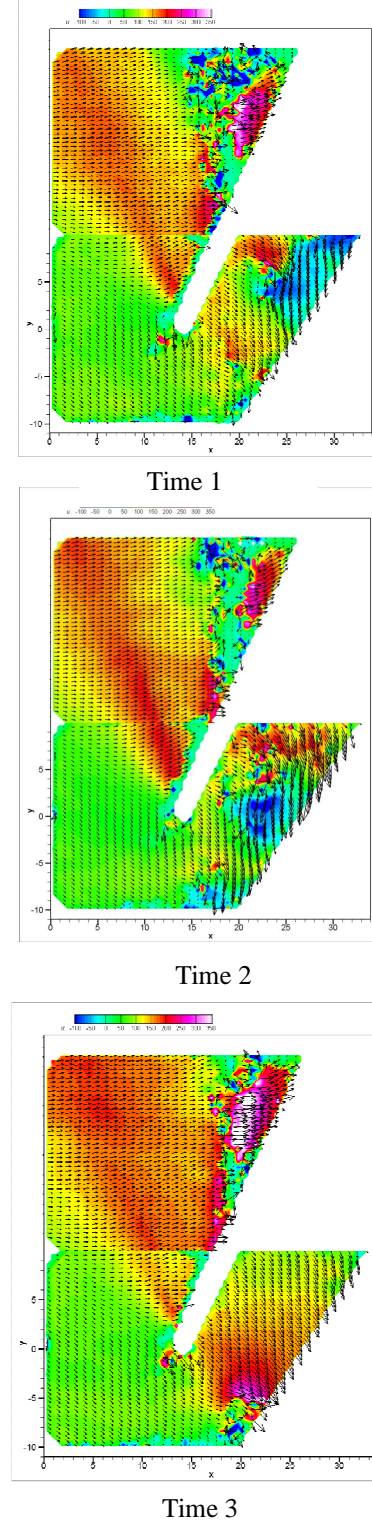


Figure 5: Changes in axial velocity at three different times from PIV measurement (Hah et al. [2010]).

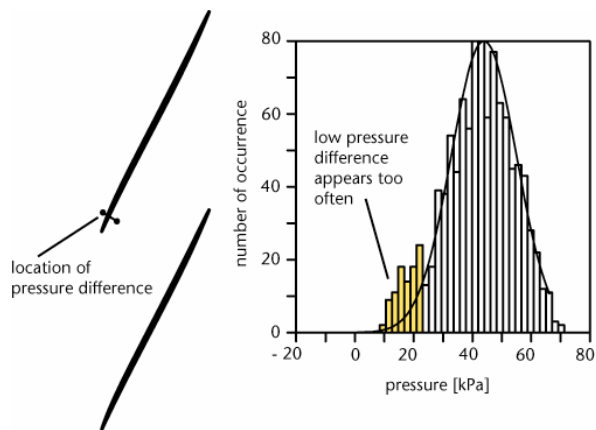


Figure 6: Changes in pressure difference across blade tip at near-stall operation.

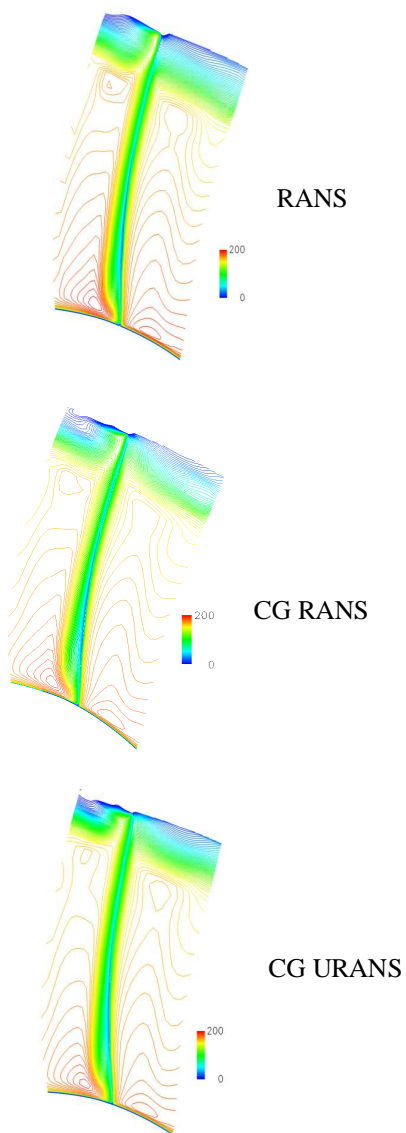


Figure 7: Axial velocity contours just downstream of trailing edge at smooth-wall stall mass flow rate.

Calculated flow structures at the blade tip are compared using static pressure distributions from RANS and time-averaged URANS, both with the CG treatment, in Figure 8. In the URANS simulation, the tip clearance vortex stays closer to the blade suction side, which further indicates less blockage accumulation in the blade passage especially near the pressure side of the blade.

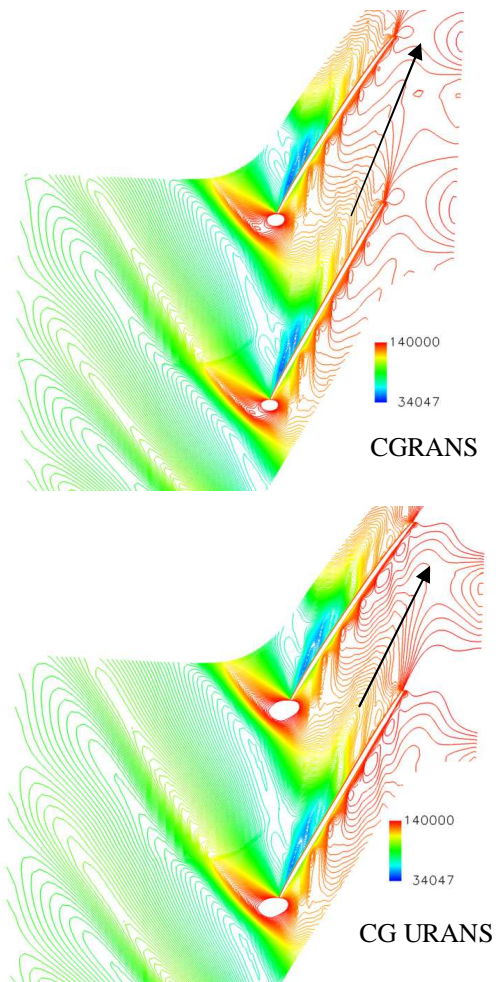


Figure 8: Static pressure distributions at casing with CG treatment from RANS and URANS at smooth-wall stall mass flow rate.

Figure 9 compares changes in RMS static pressure at the casing due to the CG casing treatment between Kulite measurements and the unsteady simulation. The measurements show that areas with very high RMS values near the pressure side of the leading edge and the shock/clearance vortex interaction area are removed by the CG casing treatment. Although the absolute levels of RMS pressure are not calculated exactly, the effects of CG on the unsteady pressure field are very well represented by the numerical simulation. This comparison in Figure 9 indicates that the current unsteady simulations do capture the major

unsteady flow phenomena fairly well for engineering applications.

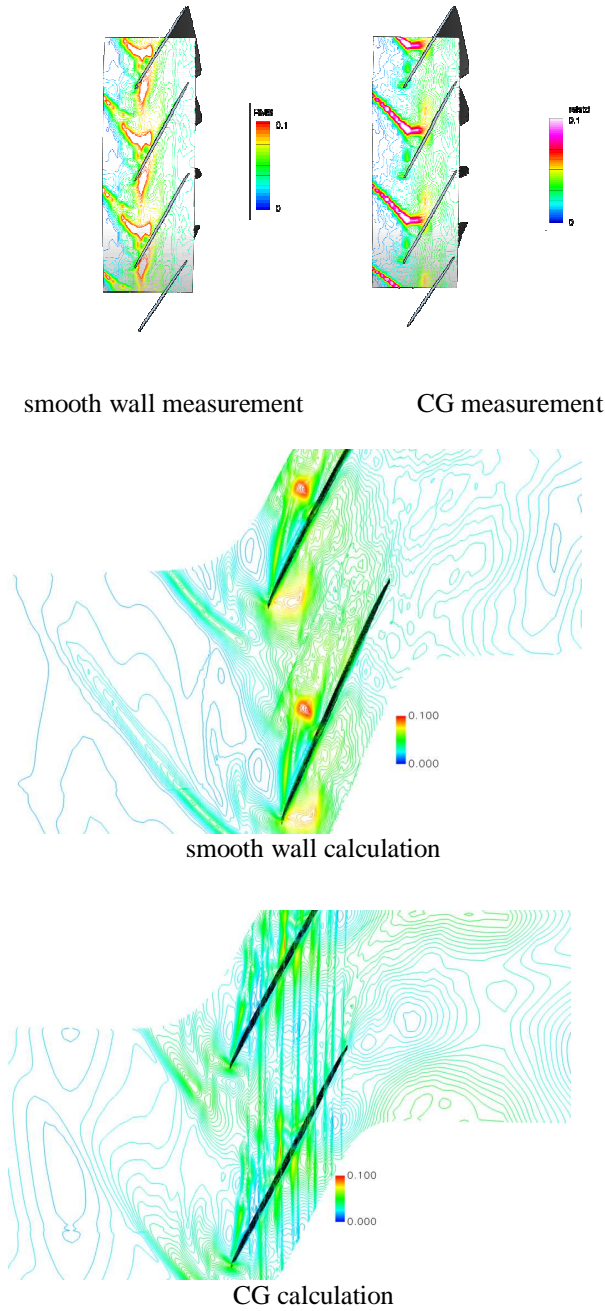


Figure 9: Comparison of RMS static wall pressure with and without CG at smooth-wall stall flow rate.

To examine flow convection into and out of the grooves, steady and unsteady radial flows near the casing are investigated using the calculated flow field and available measured data. Radial velocity component contours at 92.5% span from PIV measurements and the time-averaged URANS solution are compared in Figure 10. Calculated radial velocity at this span agrees fairly well with the PIV

measurements considering the complexity of the flow field and related uncertainties both in measurement and calculation. One interesting feature is that the measured radial velocity near the suction side of the blade points radially outward even though radially inward flow is expected near the grooves due to low pressure near the suction surface. The radially outward flow at this location might be due to the interaction with the tip clearance vortex at this location.

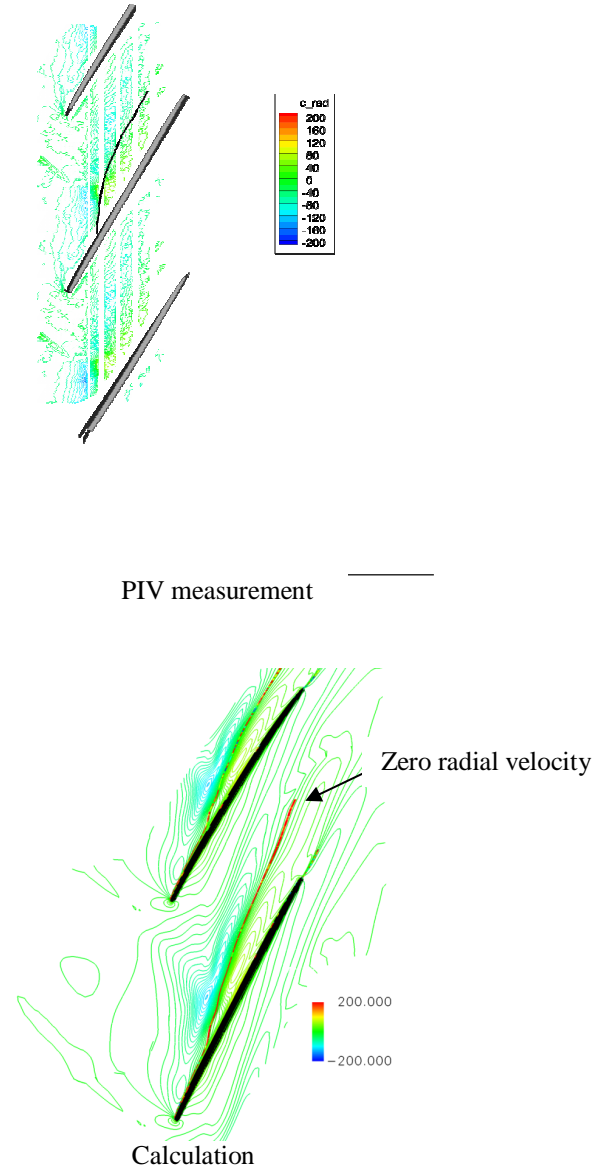


Figure 10: Comparison of radial velocity at 92.5% span with CG treatment at smooth-wall stall mass flow rate.

Calculated radial velocity contours at the blade tip (99% span) are given in Figure 11. The results in Figure 11 clearly show radially inward velocity near the suction surface as expected due to CG effects. Results in Figures 10 and 11 reaffirm the need to measure flows close to the casing and rotor tip.



Radial velocity contours at the inlet of the CG are given in Figure 12 from RANS and time-averaged URANS. Both solutions exhibit about 2.4% of the main flow going through the grooves and the distributions are very similar.

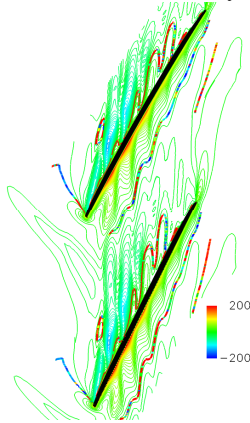
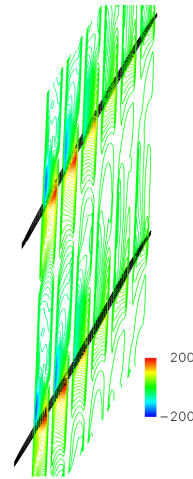
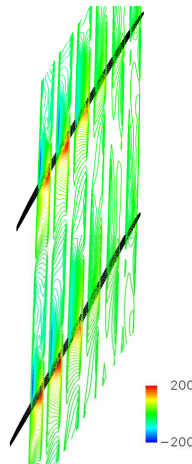


Figure 11: Calculated radial velocity at 99% span with CG treatment at smooth-wall stall mass flow rate.



RANS



URANS

Figure 12: Comparison of radial velocity contours at the inlet of grooves, smooth-wall stall mass flow rate.

RMS values of radial velocity at the blade tip section from URANS are shown in Figure 13. The maximum RMS radial velocity is 25% of the calculated time-averaged radial velocity, which implies substantial unsteady flow injection from the grooves into the main flow near the casing. The results in Figure 13 show that unsteady radial velocity is high along the path of the tip clearance vortex as expected. High RMS values are also observed below the last groove located near the trailing edge. This high RMS level indicates grooves located near the trailing edge might make a significant contribution in stabilizing the flow field through unsteady convection effects, which could not be explained with the steady RANS simulation (Rabe and Hah [2002]). This unsteady flow injection from the grooves is considered to be the main mechanism of unsteady flow convection of the CG casing treatment.

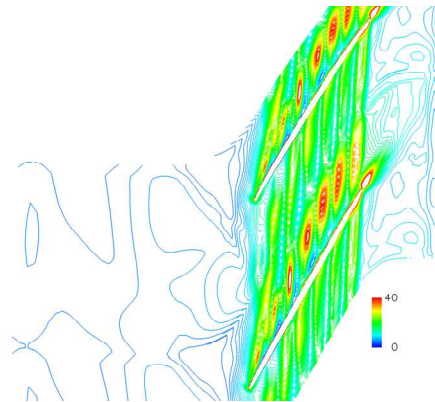


Figure 13: RMS value of radial velocity from URANS at rotor tip, smooth wall stall mass flow rate.

A recent experimental study to extend compressor stall margin by flow injection from the casing shows unsteady injection is much more effective than steady injection (Lim et al. [2011]). CG casing treatment may appear to be a steady flow device. However, flow unsteadiness at near-stall operation makes it an effective flow control device utilizing unsteady flows. The effects of unsteady flow convection in CG casing treatments is further examined in the following section by comparing flow fields calculated at the flow rate where the RANS simulation with CG treatment stalls.



## EFFECTS OF UNSTEADY FLOW INJECTION WITH THE CIRCUMFERENTIAL-GROOVE CASING TREATMENT

As shown in Figure 3, the RANS calculation yields a much higher stall mass flow than measurements for the rotor with CG casing treatment (point 4 in Figure 3). On the other hand, URANS and LES calculate lower stall mass flows than that from RANS, and hence larger improvements in stall margin.

Figure 14 compares axial velocity contours just downstream of the blade trailing edge from RANS and URANS. The results in Figure 14 again show that aerodynamic blockage from time-averaged URANS is less than that from RANS with the CG treatment. Again, the RANS and URANS simulations use the same computational grid and turbulence closure. Therefore, the difference in blockage in Figure 14 is due to unsteady effects.

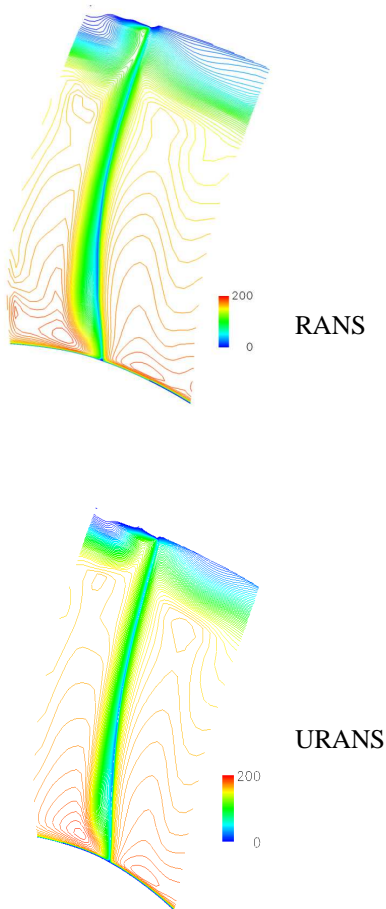


Figure 14: Comparison of axial velocity contours downstream of the trailing edge at a mass flow rate of 0.826 where RANS with CG stalls.

To examine detailed unsteady flow structures at this flow condition, LES simulations were also performed. Previous studies (for example, Hah et al [2010]) indicate that LES captures unsteady tip vortex characteristics much more realistically than URANS. This is due to the fact that the

calculated flow field from URANS has more viscous diffusion due to the single scale turbulence model

Radial velocity contours at the entrance of the CG are compared in Figure 15 from RANS and LES. The total mass going through the grooves from steady RANS is 2.4% while that from time-averaged URANS is 2.48 % and time-averaged LES is 2.5%.

RMS values of radial velocity from the LES simulation are given in Figure 16. The maximum RMS radial velocity from LES is almost 30% of the maximum mean radial velocity at this mass flow rate.

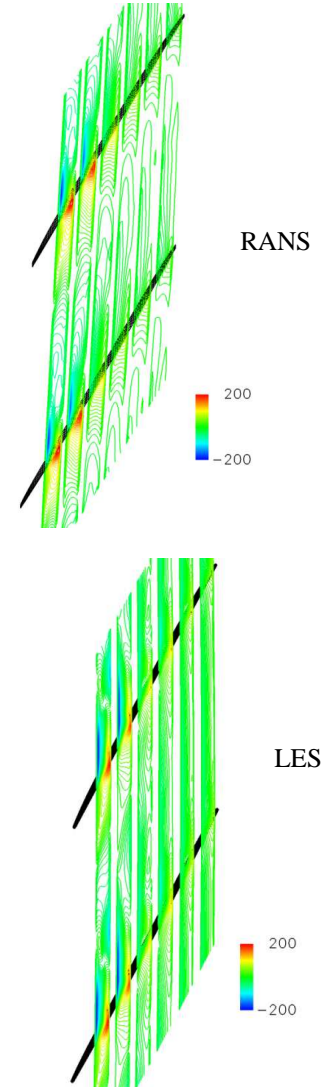


Figure 15: Comparison of radial velocity contours at the entrance of CG at mass flow rate of 0.826.

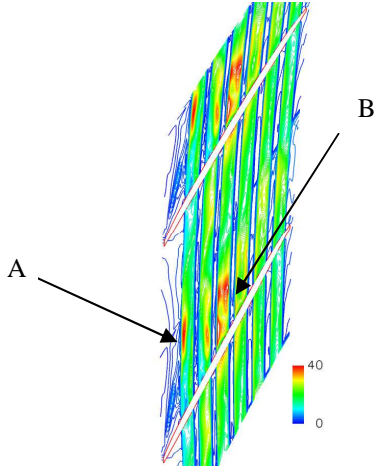


Figure 16: RMS values of radial velocity at the entrance plane of CG from LES at mass flow rate of 0.826.

A time history of axial momentum injection at the entrance of the grooves (marked as A and B in Figure 14) is given in Figure 17. The momentum is non-dimensionalized by the averaged inlet axial momentum as per Chen et al.

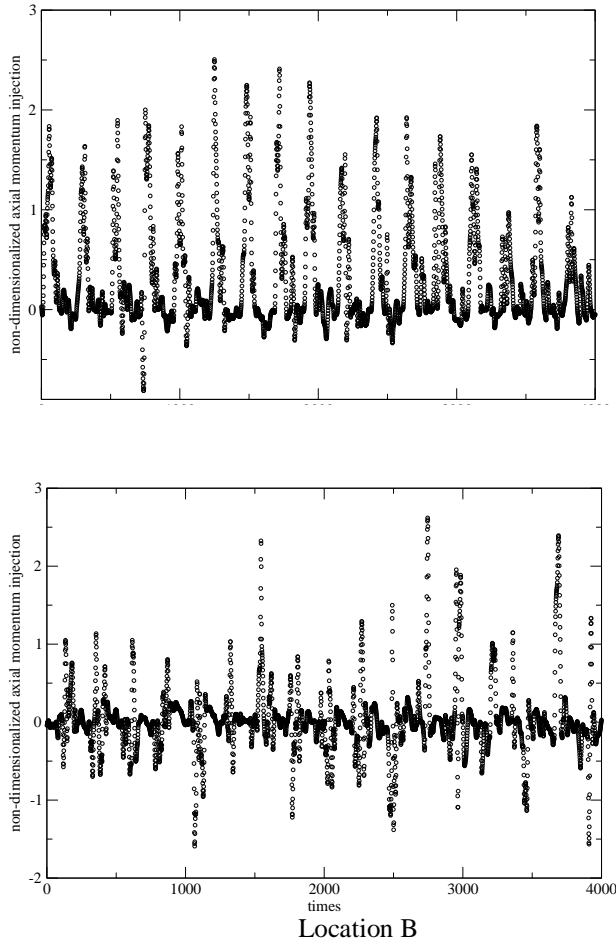


Figure 17: Unsteady injection of axial momentum from grooves at two locations at mass flow rate of 0.826.

FFT results of radial velocity at location A are given in Figure 18. A strong frequency of about one third of BPF is observed. FFT results of static pressure near blade suction surface at the rotor tip leading edge with smooth casing are given in Figure 19. The frequency in Figure 19 represents the frequency of tip clearance vortex oscillation. For this transonic rotor, the characteristic frequency of the tip clearance vortex oscillation is very similar to that of vortex shedding. Results in Figures 18 and 19 show that unsteady flow injection has the same frequency as the tip clearance vortex oscillation. Results shown in Figures 14 through 17 indicate that unsteady flow injection from the circumferential grooves is a major mechanism in extending the flow range. Results in Figure 3 show that unsteady effects are of similar magnitude as steady effects

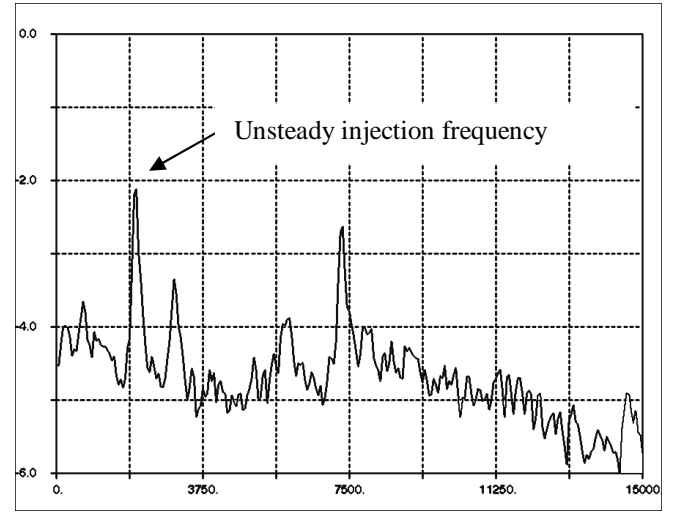


Figure 18: Spectrum of radial velocity at inlet of the first groove

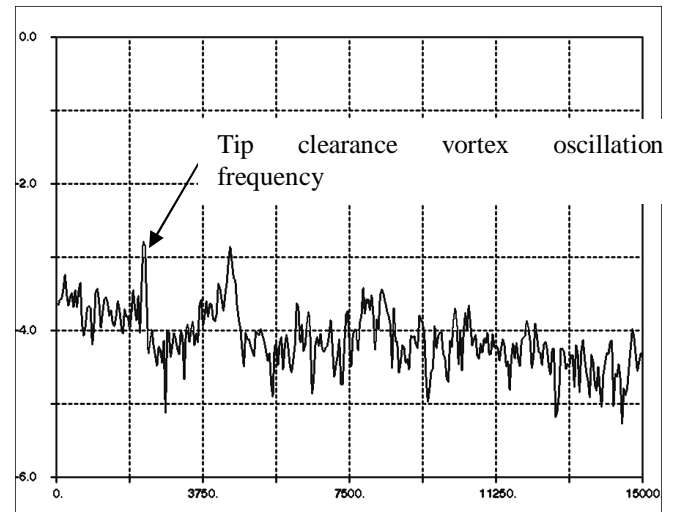


Figure 19: Spectrum of wall pressure near suction surface leading edge with smooth wall

## CONCLUDING REMARKS

The effects of steady and unsteady flow convection in a circumferential-groove casing treatment are studied in this paper. The primary motivation is that steady flow simulation of CG casing treatment does not capture measured stall margin improvements even when various limitations of a single-passage stall calculation are considered. The CG casing treatment is primarily intended to affect the flow field at near-stall operation, when the flow field is highly transient due to self-induced flow oscillation. Detailed examination of the numerical simulation of the flow fields with and without casing grooves reveals following:

1. Unsteady flow injection is the major flow mechanism of the CG casing treatment to stabilize the flow field near stall. RMS values of radial velocity into and out of the grooves are as high as 30% of the average value.
2. The unsteady flow injection has the same characteristic frequency as the tip clearance vortex oscillation.
3. The unsteady convective flow effects are of the same order of magnitude as the steady convective flow effects.

Further understanding of unsteady convective flow effects might lead to the design of advanced casing treatment devices in the future.

## REFERENCES

- Bergner, J., Matthias, K., Schiffer, H. P., and Hah, C., 2006, "Short Length-Scale Rotating Stall Inception in a Transonic Axial Compressor - Experimental Investigation," ASME Paper GT2006-90209.
- Chen, H., Huang, X., Shi, K., Fu, S., Bennington, M.A., Morris, S.C., Ross, M., McNulty, S., and Wadia, A., 2010, "A CFD Study of Circumferential Groove Casing Treatments in a Transonic Axial Compressor," ASME Paper GT2010-23606.
- Crook, A. J., Greitzer, E. M., Tan, C. S., and Adamczyk, J. J., 1993, "Numerical Simulation of Compressor Endwall and Casing Treatment Flow Phenomena," ASME Journal of Turbomachinery, Vol. 115, No. 3, pp. 501-512.
- Fujita, H. and Takata, H., 1985, "A Study of Configurations of Casing Treatment for Axial Flow Compressors," Bull. of JSME, Vol. 27, No. 230, pp. 1675-1681.
- Germano, M., Piomelli, U., Moin, P., and Cabot, W. H., 1991, "A Dynamic Subgrid-Scale Eddy-Viscosity Model," Journal of Fluid Mechanics, Vol. A3, pp. 170-176.
- Hah, C., Rabe, D. C., and Wadia, A. R., 2004, "Role of Tip-Leakage Vortices and Passage Shock in Stall Inception in a Swept Transonic Compressor Rotor," ASME Paper GT2004-53867.
- Hah, C., Voges, M., Mueller, M. W., and Schiffer, H. P., 2010, "Characteristics of Tip Clearance Flow Instability in a Transonic Compressor," ASME Paper GT-2010-22101.
- Hah, C. and Wennerstrom, A. J., 1990, "Three-Dimensional Flow Fields Inside a Transonic Compressor with Swept Blades," ASME Journal of Turbomachinery, Vol. 113, No. 1, pp. 241-251.
- Hall, E. J., Heidegger, N. J., and Delaney, R. A., 1996, "Performance Prediction of Endwall Treated Fan Rotors with Inlet Distortion," AIAA Paper AIAA 96-0244.
- Lim, H.S., Song, S.J., Kang, S.H., and Yang, S.S., 2011, "Stability Enhancement of a Low Speed Axial Compressor with Tip Injection," ISABE Paper, ISABE-2011-1207, Gothenburg, Sweden.
- Lee, N. K. W. and Greitzer, E. M., 1990, "Effects of Endwall Suction and Blowing on Compressor Stability Enhancement", ASME Journal of Turbomachinery, Vol. 122, pp. 133-144.
- Maerz, J., Hah, C., and Neise, W., 2002, "An Experimental and Numerical Investigation into the Mechanism of Rotating Instability," ASME Journal of Turbomachinery, Vol. 124, pp. 367-375.
- Moore, R. D., Kovich, G., and Blade, R. J., 1971, "Effect of Casing Treatment on Overall and Blade-Element Performance of a Compressor Rotor", NASA TN D-6538.
- Mueller, M. W., Schiffer, H. P., and Hah, C., 2007, "Effects of Circumferential Grooves on the Aerodynamic Performance of an Axial Single-Stage Transonic Compressor," ASME Paper GT-2007-27365.
- Mueller, M. W., Schiffer, H. P., Voges M. and Hah, C., 2011, "Investigation of Passage Flow Features in a Transonic Compressor Rotor with Casing Treatments," ASME Paper GT-2010-45364.
- Paulon, J. and Dehondt, D., 1982, "Influence of Casing Treatment on the Operating Range of Axial Compressors," ASME Paper 82-GT-103.
- Prince, D. C., Jr., Wisler, D. C., and Hilvers, D. E., 1974, "Study of Casing Treatment Stall Margin Improvement Phenomena," NASA CR-134552.
- Rabe, D. C. and Hah, C., 2002, "Application of Casing Circumferential Grooves for Improved Stall Margin in a Transonic Axial Compressor," ASME Paper GT-2002-30641.
- Shabbir, A. and Adamczyk, J. J., 2005, "Flow Mechanism for Stall Margin Improvement Due to Circumferential Casing Grooves on Axial Compressors," ASME Journal of Turbomachinery, Vol. 127, October 2005, pp. 708-717.
- Smith, G. D. J. and Cumpsty, N. A., 1985, "Flow Phenomena in Compressor Casing Treatment", ASME Journal of Engineering for Gas Turbines and Power, Vol. 117, pp. 532-541.
- Van de Wyer, N., Desset, F. B., Brouckaet, J F., Thomas, J-F. and Hiernaux, S., 2010, "Experimental Investigation of the Steady and Unsteady Flow Field in a Single Stage Low Pressure Axial Compressor with a Circumferential Groove Casing Treatment," ASME Paper GT2010-23474.

Vo, H. D., Tan, C. S., and Greitzer, E. M., 2005, "Criteria for Spike Initiated Rotating Stall," ASME Paper GT2005-

68374.